

FAST BEAM PROBE DEVELOPMENT FOR LONGITUDINAL BUNCH MEASUREMENTS AT UC DAVIS CROCKER NUCLEAR LABORATORY CYCLOTRON*

L. Knudson[†], E. Prebys, M. Backfish,

Crocker Nuclear Laboratory, University of California Davis, Davis, CA, USA

Abstract

The UC Davis Crocker Nuclear Laboratory (CNL) operates a 76-inch Isochronous Cyclotron dating to the 1960s. Recent experiments have revealed unexplained beam behavior, which cannot be directly measured with the current diagnostics. Direct measurements of the beam in the Cyclotron are challenging due to the harsh environment, including high radiation, strong magnetic fields, RF interference, and spatial constraints. To address this, we are developing a novel beam probe capable of resolving longitudinal bunch structure across 16 positions simultaneously. The fast beam probe consists of a segmented fast plastic scintillator array coupled via fiber optics to external Silicon Photomultipliers (SiPMs), mounted on a radially translating probe. We report on the probe's performance from in-air tests at the general-purpose beamline. The results demonstrate sub-nanosecond resolution, consistent sensitivity across channels, and clear signatures of beam dynamics, establishing the system's viability for measurements inside the CNL Cyclotron.

MOTIVATION

The CNL Cyclotron is a historic machine that has been operating since the 1960s with a wide variety of applications, including cancer treatment, radiation effects testing, air quality research, and more [1]. In recent years, interest in the isotope astatine-211 has increased, prompting CNL to commission a production process, which is described elsewhere [2]. It was determined that the optimal production area was a target, internal to the Cyclotron, using a 28 MeV alpha beam tune. A stack of Type HD-V2 Gafchromic film was placed on the end of the beam probe to destructively measure the transverse beam profile at the 25.25-inch position. The stack of film was exposed for approximately one minute by an alpha beam, resulting in a 12.7 mm radial and axial profile. The size of the measured profile was unexpected to CNL personnel and indicates significant oscillations in the Cyclotron that are not understood.

FAST BEAM PROBE CONSTRUCTION

The fast beam probe was designed around the harsh environment of the CNL Cyclotron, namely strong magnetic fields, radiation, RF interference, and spatial constraints, while being able to measure longitudinal bunches at various radial positions. The detector consists of a 4 × 4 array of fast



Figure 1: The top image shows the fast beam probe positioned in the general purpose beamline for the in-air test. The bottom image shows a rendering of the target portion of the detector, showcasing the scintillator array and fiber optics with the supporting geometry.

plastic scintillators (Eljen EJ-232Q 0.5% benzophenone) coupled to UV-VIS fused silica fibers, seen in Fig. 1, which transmit light to an Onsemi 16-channel SiPM array (Array-J) outside the Cyclotron [3–5]. Each 3 mm × 3 mm × 10 mm scintillator is optically coupled to four 2.93 m fibers, which are in turn matched one-to-one to SiPM channels. The SiPM array is actively cooled and read out using a 16+1 channel, 12-bit, 5 GS/s CAEN digitizer [6]. Full construction details and optimization considerations can be found in [7].

IN-AIR MEASUREMENT

An in-air test of the fast beam probe was performed at the CNL general purpose beamline seen in Fig. 1. The scintillator array was positioned in the beam path 10 cm away from the Kapton vacuum window, with the 3 mm × 3 mm scintillator face oriented perpendicular to the beam path. The CNL Cyclotron provided a focused beam of 67.5 MeV protons with an RF structure of 22.5 MHz. The beam current was tuned such that at most 1 particle per detector channel per bunch was present. All 16 SiPM channels and the Cyclotron

* Work supported by University of California Office of the President grant LF-20-653232 and US Department of Energy Grant DE-NA0003996
† lsknudson@ucdavis.edu

RF were digitized simultaneously over a one-minute interval to acquire approximately 40,000 events.

Content from this work may be used under the terms of the CC BY 4.0 licence (© 2025). Any distribution of this work must maintain attribution to the author(s), title of the work, publisher, and DOI.

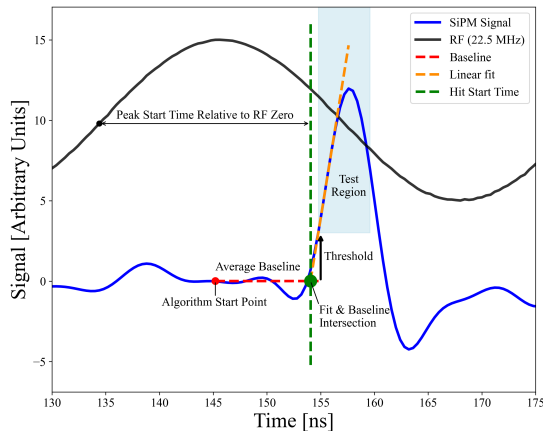


Figure 2: An example pulse event detected by the peak finding algorithm. The algorithm first calculates an average as a baseline and sets a threshold above the baseline. If all points in the test region are above the threshold, the algorithm determines that there is a valid peak. Then the first 3 points in the test region are linearly fit. The intersection between the linear fit and the baseline is defined as the global start time. The peak start time is defined by the time differential between the rising zero crossing of the RF and the global start time.

DATA ANALYSIS

Analysis was conducted following data acquisition to extract longitudinal bunch profiles. First, the SiPM traces were digitally filtered to remove low frequency noise. Then the signals were analyzed by a peak detection algorithm, seen in Fig. 2, to detect pulses in the waveform and extract timing information. After identifying a valid peak, the algorithm estimates the global start time as the intersection point between the local baseline and a linear fit to the rising edge of the pulse. The peak start time is then defined as the global start time modulo the RF phase plus an arbitrary offset¹.

Each detector channel is only sensitive to the first proton in the bunch in the transverse area, then the channel is dead for 15 ns. If we assume at most one proton impacts the detector channel per bunch, then the proton in the bunch represents a statistical sample of the longitudinal distribution of the bunch. Therefore, a collection of the peak start times from the detector forms a distribution that corresponds to the longitudinal time structure of the beam in the detector channel region.

The digitizer samples all detector channels and the RF signal to acquire 1023 events over approximately 0.75 seconds,

then the digitizer transfers the data over another 0.75 seconds and is considered dead at that time. This data structure creates a convenient bin size, a data block, to understand the longitudinal distribution being measured. Assuming that the measured distribution is Gaussian, we may fit the data block to obtain a mean, amplitude, and width to characterize the distribution (such as in Figs. 3 and 4).

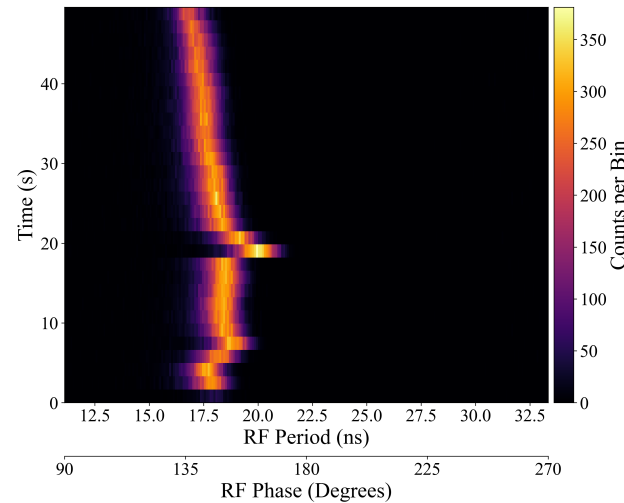


Figure 3: A 2D histogram of pulse start times (relative to the rising zero crossing of the RF) for channel 7 within a data collection window of 50 seconds. The bottom axis shows time within one RF period (22.5 MHz, 44.4 ns), while the sub axis maps this time to RF phase in degrees. The data shows fast shifts in pulse start time near the 5-second and 20-second region, stability from 10 to 18 seconds, and a slow drift from 22 seconds to the end of the data set.

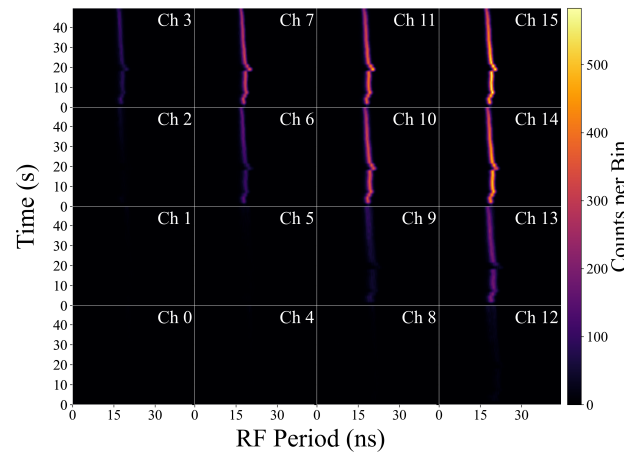


Figure 4: A 2D histogram of the measured pulse start times for all detector channels with relative physical positions preserved in the plot grid. Similar features are seen across all channels, with the relative intensity increasing towards the upper right of the detector array due to beam targeting.

¹ The arbitrary phase offset is constant for each channel in a data set and may be applied digitally or physically. The physical phase offset may not be equal between channels; a more detailed analysis of the detector is needed to extract offsets between each channel.

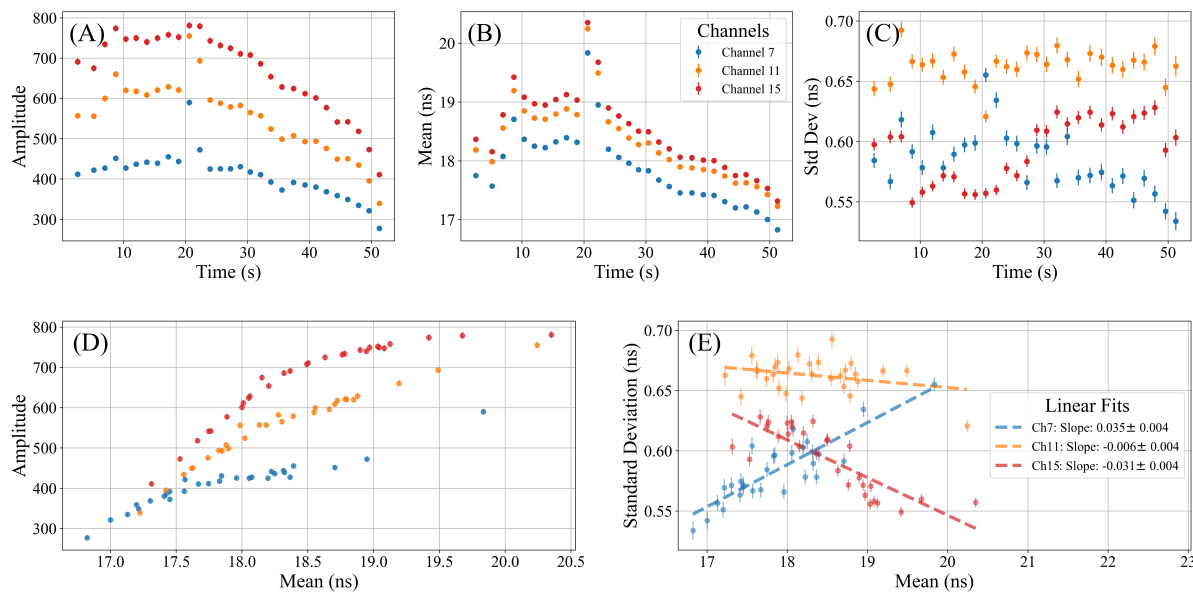


Figure 5: (A), (B), and (C) show the Gaussian fit parameters, with error bars, for each data block plotted against time. (D) and (E) are scatter plots of the amplitude and standard deviation plotted against the mean, indicating phase dependence on the fit parameters. A linear fit is calculated in plot (E), demonstrating a dependence on the standard deviation across the mean that is not shared between channels.

RESULTS

The in-air test of the fast beam probe successfully demonstrated its ability to detect and resolve the longitudinal structure of individual beam bunches. Using the pulse start time extraction method described in Fig. 2, distributions of arrival times were measured and analyzed across all 16 detector channels.

A time-resolved 2D histogram of pulse start times for channel 7 is shown in Fig. 3. This plot shows clear temporal shifts in the longitudinal phase, demonstrating the detector's sensitivity to time-dependent changes in beam structure. The same analysis was applied to all 16 channels seen in Fig. 4 with each channel represented following the physical channel layout. Phase shift trends are observed consistently across channels. Signal intensity varies due to beam alignment, with higher intensities concentrated in the upper right region of the array.

The pulse start time distributions for each channel were fit to a Gaussian within each data block to characterize the measurements over time. Fig. 5 summarizes these results for channel 7, channel 11, and channel 15. Subplots (A), (B), and (C) show the evolution of the fit parameters (mean, amplitude, and standard deviation) as a function of time. Subplots (D) and (E) display correlations between the fit parameters. All three channels demonstrate a positive correlation between the mean and the amplitude shown in (D). In (E), a linear trend is visible between the mean phase and the standard deviation, suggesting that there may exist phase dependence on the longitudinal width of the beam. Furthermore, the trend is not consistent across channels, indicating that the detector is sensitive to transverse variances.

CONCLUSION

The fast beam probe is being developed to address the lack of diagnostics in the challenging environment of the CNL Cyclotron. This testing demonstrated its ability to resolve the longitudinal structure of the beam with sub-nanosecond resolution across 16 channels. Consistent features and transverse variations observed across the array confirm the detector's sensitivity to beam dynamics. The measurements presented here show several unknown features of the beam and the capability of the fast beam probe to resolve them.

REFERENCES

- [1] Crocker Nuclear Laboratory (CNL), <https://crocker.ucdavis.edu>
- [2] E. Prebys, M. R. Backfish, D. A. Cebra, R. B. Kibbee, L. M. Korkeila, and K. S. Stewart, "First Production of Astatine-211 at Crocker Nuclear Laboratory at UC Davis", in *Proc. IPAC'22*, Bangkok, Thailand, Jun. 2022, pp. 3038–3040.
doi:10.18429/JACoW-IPAC2022-THPOMS035
- [3] Eljen Technology, <https://eljentechnology.com/products/plastic-scintillators/ej-232-ej-232q>
- [4] SitusLight, <https://situslight.com/2023/04/optical-fibers/>
- [5] Onsemi, <https://www.onsemi.com/download/data-sheet/pdf/microj-series-d.pdf>
- [6] Caen, <https://www.caen.it/products/dt5742/>
- [7] L. Knudson, E. Prebys and M. Backfish, "Fast cyclotron beam probe at UC Davis Crocker Nuclear Laboratory", in *Proc. IPAC'25*, Taipei, Taiwan, Jun. 2025, pp. 2770-2772.
doi:10.18429/JACoW-IPAC25-THPM039